Computational Materials Science 80 (2013) 2–14

Contents lists available at SciVerse ScienceDirect

Computational Materials Science

journal homepage: www.elsevier.com/locate/commatsci

A parameter study of intercalation of lithium into storage particles in a lithium-ion battery

Rajlakshmi Purkayastha [a], Robert McMeeking [a,b,c,d,*]

[a] Materials Department, University of California, Santa Barbara, CA 93106, United States
[b] Department of Mechanical and Environmental Engineering, University of California, Santa Barbara, CA 93106, United States
[c] School of Engineering, Aberdeen University, King's College, Aberdeen AB24 3UE, Scotland, United Kingdom
[d] INM – Leibniz Institute for New Materials, Campus D2 2, D-66123 Saarbrücken, Germany

ARTICLE INFO

Article history:
Received 5 November 2011
Received in revised form 29 March 2012
Accepted 23 November 2012
Available online 29 January 2013

Keywords:
Intercalation
Lithium-ion batteries
Stress maps
Coupled diffusion-stress model

ABSTRACT

The effect of stress on storage particles within a lithium ion battery, while acknowledged, is not fully understood. In this study we identify three non-dimensional parameters which govern the stress response within a spherical storage particle, and we carry out numerical simulations to characterize the stresses that are developed. The non-dimensional parameters are developed using system properties such as the diffusion coefficient, particle radius, lithium partial molar volume and Young's modulus. Stress maps are generated for various values of these parameters for fixed rates of insertion, with boundary conditions applied to particles similar to those found in a battery. Stress and lithium concentration profiles for various values of these parameters show that the coupling between stress and concentration is magnified depending on the values of the parameters. The resulting maps can be used for different materials, depending on the value of the dimensionless parameters. Finally, the value of maximum stress generated is calculated for extraction of lithium from the particle and compared with those generated during insertion.

1. Introduction

As battery technologies are being applied to large scale portable devices e.g. automobiles, it is being realized that the ageing and subsequent failure of the battery are not very well understood. The US government has specified a list of requirements [1] for use in electric vehicles, one of which is an extended lifetime of 10–15 years. Ageing manifests primarily as decrease in capacity or capacity fade, power fade, increase in impedance and an overall decrease in performance [2–4].

In Fig. 1 we see a schematic of a lithium ion battery. There are two different electrodes, the anode and the cathode, which are each connected to a metal plate called the current collector. A dividing polymeric segment known as the separator lies in between the two electrodes. Within the electrodes themselves there are storage particles. For the cathode, these consist of layered materials or oxides, such as lithium manganate and lithium cobalt oxide. For the cathode the most conventional material in use is graphite, or some form of carbon. The storage particles are mixed along with a polymeric binder, e.g. PVDF, which is added to give the structure integrity, along with carbon particles which are added in order to boost the electronic conductivity. Finally the entire electrode and separator is filled with the electrolyte. This normally consists of a lithium-based ionic salt, e.g. $LiPF_6$, dissolved in an organic solvent.

During the discharge process, i.e. extraction of electrical energy from the battery, lithium stored in the anode is oxidized to its ionic form and moves through the electrolyte to the cathode. The electrons flow through the external circuit as they cannot pass through the electrolyte in the separator. The electrons flow into the storage particle in the cathode through the current collector. The lithium ions recombine with the electrons and remain in the storage particle in the cathode. During the charging process the reverse occurs, with lithium leaving storage particles in the cathode and moving into storage particles in the anode.

The process of removing or inserting lithium ions into the storage particles is known as intercalation. This can be formally defined as the insertion of a guest species into normally unoccupied interstitial sites in the crystal structure of an existing stable host material [2]. Though the chemical composition of the host phase initially present can be substantially modified, the basic crystal structure is preserved. The addition of interstitial species causes a change in volume: this leads to strain, and, when it is heterogeneous, stress in the system.

This shrinking and swelling of storage particles can lead to comminution of the particles. Depending on the material being used as

* Corresponding author. Address: Department of Mechanical and Environmental Engineering, University of California, Santa Barbara, Santa Barbara CA 93106, United States. Tel.: +1 805 893 8434.
E-mail address: rmcm@engineering.ucsb.edu (R. McMeeking).

0927-0256/$ - see front matter © 2012 Elsevier B.V. All rights reserved.
http://dx.doi.org/10.1016/j.commatsci.2012.11.050

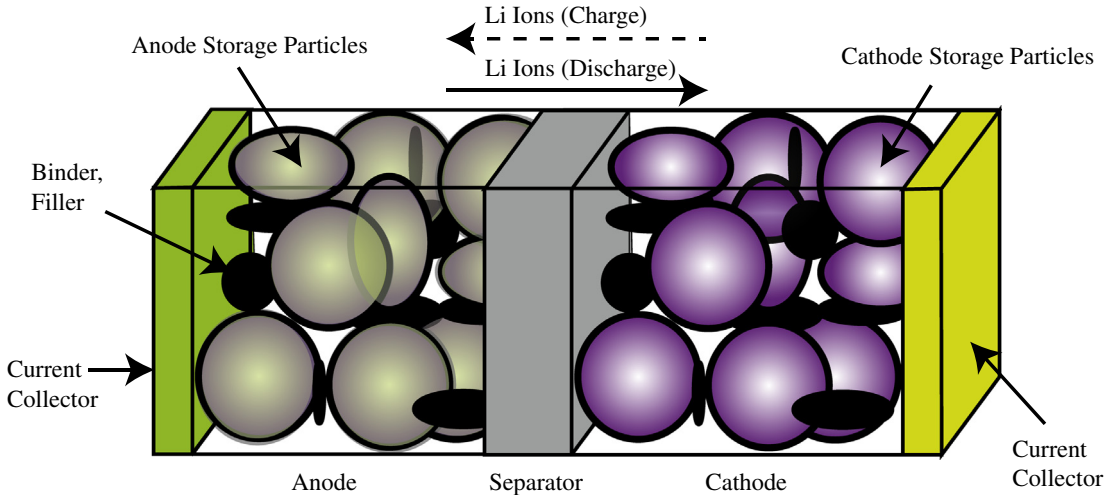

Fig. 1. A schematic of the structure of the lithium ion battery. The main components are the current collectors, the electrodes, the anode and cathode and the separator. The electrodes are made up of active storage particles, binder and filler. Electrolyte fills the pores of the structure, including both electrodes and the separator. The particles in an actual battery are not so regular in shape, but for the purposes of our simulation they are spherical. Lithium ions flow through the separator from the anode to the cathode during discharge and vice versa during the charging process.

much as 100% of the lithium can be extracted, which leads to significant shrinkage [5]. In $LiMn_2O_4$ it is observed that a depletion of around 60% of the original capacity leads to a volume reduction of 6.5% [6]. During charging, lithium in the cathode intercalates initially from the surface of the storage particle, leading to a high tensile hoop stress there as the outer layer shrinks. This can lead to comminution of the particle during charging [3], which is aggravated over repeated cycling of the battery. Graphite, an anode material, is observed to show an increase in volume by 8% when the number of lithium atoms per C ring is increased from 0 to 0.6 [6]. Of further concern are newer materials such as Si which can swell by almost 300% [4,7,8]. Such materials will therefore show significant stress and strain generation during cycling of the battery, and will hamper their use on a large scale.

Porous electrode theory [9] has been extensively used to represent the complex microstructure of the battery as a 1-d approximation [6,8,10–14]. This has lead to 'pseudo-2D' models, in which a single particle is coupled to a battery simulator based on porous electrode theory [15,16] and models have now been refined to include phase transformations as well. Garcia et al. [17,18] studied stresses within the electrode using a 2-D model, in which the entire electrochemistry of the battery was modeled including storage particles, binder and electrolyte pores. However, these results are highly dependent on the material data that is observed from experiments.

Single particle models have been used to examine what occurs within the particle in much more detail with stress and diffusion coupled. Christensen and Newman [6] developed a multi-component diffusion model for estimating the stress generated in $Li_xMn_2O_4$, where they included the volume change during phase change. The pressure term was used to account for the stress generated within the particle. Sastry and workers [19] developed a model based on a thermal analogy for stress, and also took into account the effect of different shapes of the particle as well as phase changes [20]. Verbrugge and Cheng [21,22] developed analytical models for stress within the particle for calculating the diffusion induced stresses (DIS) based on the concentration within the particle, i.e. the stress is coupled to the concentration but not vice versa. Bohn [23] developed a simulation for the diffusion within the particle based on a model for the Li chemical potential encompassing excess Gibbs free energy. As a result they are able to simulate the effect of phase change and staging in the storage particles.

Previous work has shown that the storage particles within the battery electrodes develop cracks over time and eventually comminute [24–27]. There have been several attempts at applying fracture mechanics to these problems in order to predict conditions conducive to cracking [28–32] and criteria suggested to avoid it [33–36].

A common theme running through all of these studies is that they are material specific. The complications which arise while taking all the material parameters and their concentration dependence into account can sometimes obscure the result. Moreover, no property maps are developed which are generic, i.e. that can be used across a variety of materials. A map for the stress as a function of the discharge rate and particle radius has been provided for lithium manganate and graphite in [23], while fracture maps have been developed for lithium manganate [33], lithium iron phosphate [36] and lithium cobalt oxide [30].

In this paper we aim to develop such property maps in order to identify the parameters which determine the stress response within storage particles for a variety of materials. We first develop a model for diffusion based on the work of Bohn [23]. The equations are then non-dimensionalized and three dimensionless parameters of influence are identified. Stress maps for insertion of lithium into the particle are then plotted, and the results are analyzed and explained. Finally, a comparison of results is made with those from extraction studies.

2. Methodology

In this section the model for the coupled diffusion-stress model is modified and non-dimensionalized. We consider the particle to be spherical in shape. Although in an actual electrode the particles do not have a regular shape, it is prudent to consider a regular shape initially for ease of calculations. The resulting analysis will also be clearer and help in our understanding of the coupling between the stress and concentration profiles.

2.1. Theory and equations

Bohn [23] developed an equation for chemical potential of lithium per mole when it is intercalating a storage particle. The following assumptions are used to arrive at Eq. (1).

(i). The intercalation solution is assumed to be ideal.

(ii). The storage particle expands and contracts isotropically during intercalation/de-intercalation of lithium.
(iii). The strain is small and thus the mechanics of infinitesimal straining can be applied.
(iv). The partial molar volume is assumed to be independent of lithium concentration.
(v). There is no interaction between lithium ions in the storage particle; i.e. the excess Gibbs free energy is taken to be zero.

$$\mu_{Li} = \mu_{Li}^0 + RT\ln\frac{c_{Li}}{c_{\max} - c_{Li}} - \Omega_{Li}\sigma_h \quad 0 \leqslant c_{Li} \leqslant c_{\max} \tag{1}$$

μ_{Li}^0 is the ideal enthalpic contribution per mole of lithium when dissolved in the lattice. The 2nd term on the right hand side is a model for the ideal entropic contribution. The contribution of mechanical energy is given by $-\Omega_{Li}\sigma_h$, where Ω_{Li} is the partial molar volume of lithium dissolved in the lattice and σ_h is to the hydrostatic stress within the particle. c_{Li} is the concentration of lithium in moles per unit volume, and $c_{\max}$ is the maximum possible concentration of lithium dissolved in a storage particle. We assume that the host material has a finite number of sites for lithium intercalation for a particular phase. On addition of lithium beyond $c_{\max}$ further intercalation sites are unavailable and a new phase must form.

The vector flux, J_{Li} of lithium within the particle, in moles per unit area per unit time, is given by

$$J_{Li} = c_{Li} v_{Li} \tag{2}$$

where v_{Li} is the vector of average velocity of lithium, proportional to its mobility, M_{Li}, and the gradient of its chemical potential, so that

$$J_{Li} = -c_{Li} M_{Li} \nabla \mu_{Li} \tag{3}$$

Following [23], the mobility is taken to be isotropic and a function of lithium concentration. As the concentration of lithium increases the likelihood of a successful hop from one intercalation site to another decreases, so that

$$M_{Li} = M_0\left(1 - \frac{c_{Li}}{c_{\max}}\right) \tag{4}$$

where the parameter, M_0, is given by

$$D_0 = M_o RT \tag{5}$$

with D_o the concentration independent diffusion parameter. Thus at $c_{\max}$, there are no sites for lithium to intercalate into and $M_{Li} \to 0$.

On combining Eq. (1)–(4), the flux is given by

$$J_{Li} = -D_0\left\{\nabla c_{Li} - \left(1 - \frac{c_{Li}}{c_{\max}}\right)\frac{\Omega_{Li} c_{Li}}{RT}\nabla\sigma_h\right\} \tag{6}$$

In the absence of the stress gradient term the equation becomes equivalent to Ficks diffusion law, i.e. the flux is proportional the gradient of the concentration. The inclusion of the stress gradient arises from the rigorous derivation of the chemical potential and mobility, and we can conclude the Eq. (6) is also rigorous. An important difference between this formulation and that of Zhang et al. [19] is the presence of the term $(1 - c_{Li}/c_{\max})$. Bohn [23] notes that this term brings symmetry into the effect of the hydrostatic stress gradient on the overall lithium flux. Thus the effect of stress will be similar both when $c_{Li} \to 0$ and $c_{Li} \to c_{\max}$. At both extremes of concentration the contribution of the stress gradient will be zero. This occurs because entropy effects dominate the lithium chemical potential at these concentrations rendering the effect of the hydrostatic stress negligible.

Other formulations for lithium diffusion in a storage particle include those derived using multi-component diffusion [6,15] where a pressure term accounts for the effects of stress. This is consistent with our set-up with a few differences in the details. In some formulations the stress and concentration are not directly coupled [20,21,31,34,35] while in others the interaction of lithium ions is also taken into account using non-ideal thermodynamics [6,23,37]. Activity coefficients for these can be derived using the open circuit potential (OCP) of the electrode material [6,23].

From conservation of mass we get

$$\frac{\partial c_{Li}}{\partial t} + \nabla \cdot J_{Li} = 0 \tag{7}$$

Combining Eqs. (6) and (7) we obtain

$$\frac{\partial c_{Li}}{\partial t} = D_0 \nabla \cdot \left\{\nabla c_{Li} - \left(1 - \frac{c_{Li}}{c_{\max}}\right)\frac{\Omega_{Li} c_{Li}}{RT}\nabla\sigma_h\right\} \tag{8}$$

Swelling strains that occur as a result of volume change brought about by intercalation/de-intercalation of lithium into the storage particle are considered in Eq. (9). The total strain accounts for elastic contributions that arise since the swelling strains are heterogeneous.

$$\varepsilon = \frac{1}{E}[(1+\nu)\sigma - 3\nu\sigma_h I] + \frac{\Omega_{Li}(c_{Li} - c_0)}{3} I \tag{9}$$

ε is the strain tensor, E is Young's modulus, ν is Poisson's ratio, I is the identity tensor and c_0 is a datum concentration at which the swelling strain is considered to be zero. The equation for equilibrium of stress is given by

$$\nabla \cdot \sigma = 0 \tag{10}$$

Given that the free surface of the storage particle is traction free, the result for thermal stresses in a solid spherical body of outer radius r_0 when the temperature distribution is spherically symmetric, as derived by Timoshenko and Goodier [38] and utilized by Zhang et al. [19], is used. The radial, σ_r and circumferential, σ_c, stresses are given by

$$\sigma_r = \frac{2\Omega_{Li}E}{3(1-\nu)}\left(\frac{1}{r_0^3}\int_0^{r_0} c_{Li} r^2 dr - \frac{1}{r^3}\int_0^{r} c_{Li} r^2 dr\right) \tag{11}$$

$$\sigma_c = \frac{\Omega_{Li}E}{3(1-\nu)}\left(\frac{2}{r_0^3}\int_0^{r_0} c_{Li} r^2 dr + \frac{1}{r^3}\int_0^{r} c_{Li} r^2 dr - c_{Li}\right) \tag{12}$$

where r is measured from the center of the particle. The hydrostatic stress is given by

$$\sigma_h = \frac{\sigma_r + 2\sigma_c}{3} = \frac{2\Omega_{Li}E}{3(1-\nu)}\left(\frac{1}{r_0^3}\int_0^{r_0} c_{Li} r^2 dr - \frac{c_{Li}}{3}\right) \tag{13}$$

From these equations, it can be determined that, during steady insertion starting from uniform lithium concentration, the maximum principal stress is tensile, occurs at the center of the particle, and is given by

$$\sigma_{\max}(t) = \frac{2\Omega_{Li}E}{3(1-\nu)}\left[\frac{1}{r_0^3}\int_0^{r_0} c_{Li}(r,t) r^2 dr - \frac{c_{Li}(0,t)}{3}\right] \tag{14}$$

Note that at the center of the particle, the stress is purely hydrostatic, so that the maximum principal stress in this case is any of the 3 stress components at the particle center. During steady extraction starting from uniform lithium concentration, the maximum principal stress is circumferential, tensile, occurs at the particle surface, and is given by

$$\sigma_{\max}(t) = \frac{\Omega_{Li}E}{3(1-\nu)}\left[\frac{3}{r_0^3}\int_0^{r_0} c_{Li}(r,t) r^2 dr - c_{Li}(r_0,t)\right] \tag{15}$$

2.2. Boundary and initial conditions

Earlier simulations, for both insertion and extraction of lithium from a storage particle, used two types of boundary conditions. The particle initially has a uniform concentration (0 or $c_{\max}$ for the case

of insertion or extraction). In the first scenario, a steady state flux is applied to the surface of the particle, i.e. galvanostatic charging/discharging. The concentration at the surface will reach either extreme of concentration (0 or c_{max}) [6,19,20–23] and the simulation is stopped. In the second scenario, the single particle is coupled to a battery simulator, e.g. Dualfoil [6,8–11]. The simulator mimics the boundary conditions that exist at the surface of the particle as a function of the potential and concentration of the surrounding electrolyte using Butler–Volmer kinetics. It can therefore predict the flux at the particle surface as a function of electrode thickness and time. Thus the simulation can be run beyond the steady state insertion stage, and more realistic conditions can be created. For example in a battery, after galvanostatic charging is carried out until a certain concentration is attained, the electrode is held at a constant potential for some time to equalize the concentration of the lithium, i.e. potentiostatic charging.

We wish to simulate conditions closer to those used in practice, without resorting to using a battery simulator. We replicate these conditions by doing the following

i. In the case of insertion, the particle has a uniform initial lithium concentration $c_{Li} = 0$. It is charged galvanostatically, with uniform lithium flux through its entire free surface, until the surface reaches the maximum permitted lithium concentration, i.e. until $c_{Li}(r_0, t) = c_{max}$. Thereafter, the concentration at the particle surface is held fixed at $c_{Li}(r_0, t) = c_{max}$ while the insertion process continues. The simulation can be continued for an arbitrary time, but for practical reasons we terminate insertion when the average value of c_{Li}/c_{max} within the particle becomes equal to 0.99. Note that the average value of c_{Li}/c_{max} in the negative electrode is known as the state of charge (SOC). We will adopt this terminology for individual storage particles indiscriminately, using the term SOC as defined above for any storage particle, notwithstanding whether it is for the positive or negative electrode.
ii. Extraction is treated similarly. In this case the initial SOC is 1.0 and the lithium concentration in the particle is uniform. The lithium is extracted galvanostatically with uniform flux through the particle surface until the lithium concentration at the surface is zero, i.e. until $c_{Li}(r_0, t) = 0$. Thereafter, the concentration at the particle surface is held fixed at $c_{Li}(r_0, t) = 0$ while the insertion process continues. For practical reasons, we terminate the simulation when the SOC becomes equal to 0.01.

The point at which the boundary conditions are changed from galvanostatic charging to potentiostatic charging is referred to as the transition point. This procedure is quite close to the boundary conditions as applied using a battery simulator (Butler–Volmer kinetics). During galvanostatic lithium insertion or extraction, the exchange current density and the surface overpotential do not change greatly, consistent with a steady lithium flux at the surface of the particle. When the lithium concentration at the particle surface reaches its extreme (i.e. $c_{Li}(r_0, t) = 0$ or $c_{Li}(r_0, t) = c_{max}$), the surface overpotential and exchange current density adjust in such a way that the lithium concentration at the particle surface remains close to its extreme value (i.e. close to $c_{Li}(r_0, t) = 0$ or close to $c_{Li}(r_0, t) = c_{max}$), a result that comes about because of the tendency for side reactions to become dominant and because the Gibbs free energy of the new phases that develop beyond these extremes is relatively high.

Furthermore, the surface concentration of lithium in the storage particle determines the lithium chemical potential there (at least in the absence of stress at the free surface, see Eq. (1)). Note that the OCP of the particle surface is directly related to the lithium chemical potential by

$$FU^s(t) = \tilde{\mu}_{Li} - \mu_{Li}(r_0, t) \tag{16}$$

where $\tilde{\mu}_{Li}$ is the lithium chemical potential in the reference electrode used to define the OCP for the electrode within which the given storage particle lies. Thus when a constant potential is applied to a battery, the potentials of the electrolyte and the particle at its surface adjust in order to achieve steady values. A constant potential imposed at the particle surface is thus equivalent to holding the lithium concentration fixed. In summary, we are therefore modeling the effects on a storage particle during battery charging and discharge as a galvanostatic process taking the surface lithium concentration from one extreme value to another (i.e. from $c_{Li}(r_0, t) = 0$ to $c_{Li}(r_0, t) = c_{max}$ or from $c_{Li}(r_0, t) = c_{max}$ to $c_{Li}(r_0, t) = 0$) followed by a potentiostatic process in which the surface lithium concentration is held fixed (i.e. at $c_{Li}(r_0, t) = 0$ or at $c_{Li}(r_0, t) = c_{max}$).

2.3. Non-dimensionalization

To ensure that the study is generic and applicable to a wide range of materials, battery designs and performance indicators, the equations are non-dimensionalized. Following Zhang et al. [19] we use the non-dimensionalized position, time, lithium concentration and surface current density given by

$$\hat{r} = \frac{r}{r_0} \quad \hat{t} = \frac{tD_0}{r_0^2} \quad \hat{c}_{Li} = \frac{c_{Li}}{c_{max}} \quad \widehat{I} = \frac{i_n r_0}{FD_0 c_{max}} \tag{17}$$

The stress tensor is normalized by the Young's modulus so that the result represents the scale of the elastic strains. A new parameter is introduced as the non-dimensionalized partial molar volume so that

$$\hat{\sigma} = \frac{\sigma}{E} \quad \widehat{\Omega} = \frac{\Omega_{Li} E}{RT} \tag{18}$$

Note that there is an additional non-dimensional parameter, namely Poisson's ratio, ν.

In non-dimensional form, the diffusion equation for lithium transport in the storage particle reduces to

$$\frac{\partial \hat{c}_{Li}}{\partial \hat{t}} = \left(\frac{\partial}{\partial \hat{r}} + \frac{2}{\hat{r}}\right)\left[\frac{\partial \hat{c}_{Li}}{\partial \hat{r}} - \widehat{\Omega}(1 - \hat{c}_{Li})\hat{c}_{Li}\frac{\partial \hat{\sigma}_h}{\partial \hat{r}}\right] \tag{19}$$

During the galvanostatic stage of the process, the boundary condition is

$$\frac{\partial \hat{c}_{Li}(1, \hat{t})}{\partial \hat{r}} = -\widehat{I} + \widehat{\Omega}(1 - \hat{c}_{Li})\hat{c}_{Li}\frac{\partial \hat{\sigma}_h(1, \hat{t})}{\partial \hat{r}} \tag{20}$$

whereas in the potentiostatic stage the boundary condition is

$$\hat{c}_{Li}(1, \hat{t}) = 1 \tag{21}$$

during insertion and

$$\hat{c}_{Li}(1, \hat{t}) = 0 \tag{22}$$

during extraction. The formulae for hydrostatic stress, Eq. (15) can be stated in non-dimensional form.

$$\hat{\sigma}_h = \frac{2\varepsilon_{Li}^{max}}{3(1-\nu)}\left(\int_0^1 \hat{c}_{Li}\hat{r}^2 d\hat{r} - \frac{\hat{c}_{Li}}{3}\right) \tag{23}$$

where

$$\varepsilon_{Li}^{max} = \Omega_{Li} c_{max} \tag{24}$$

is the final dimensionless parameter, representing the maximum swelling strain that can be induced by the lithium.

The model is implemented using the finite element method using the commercial code COMSOL [39]. The three irreducible parameters $\widehat{I}$, $\widehat{\Omega}$ and ε_{Li}^{max} can be used to generate solutions for particle stress and SOC. Zhang et al. [19] published a plot for the maximum principal stress during lithium galvanostatic insertion as a

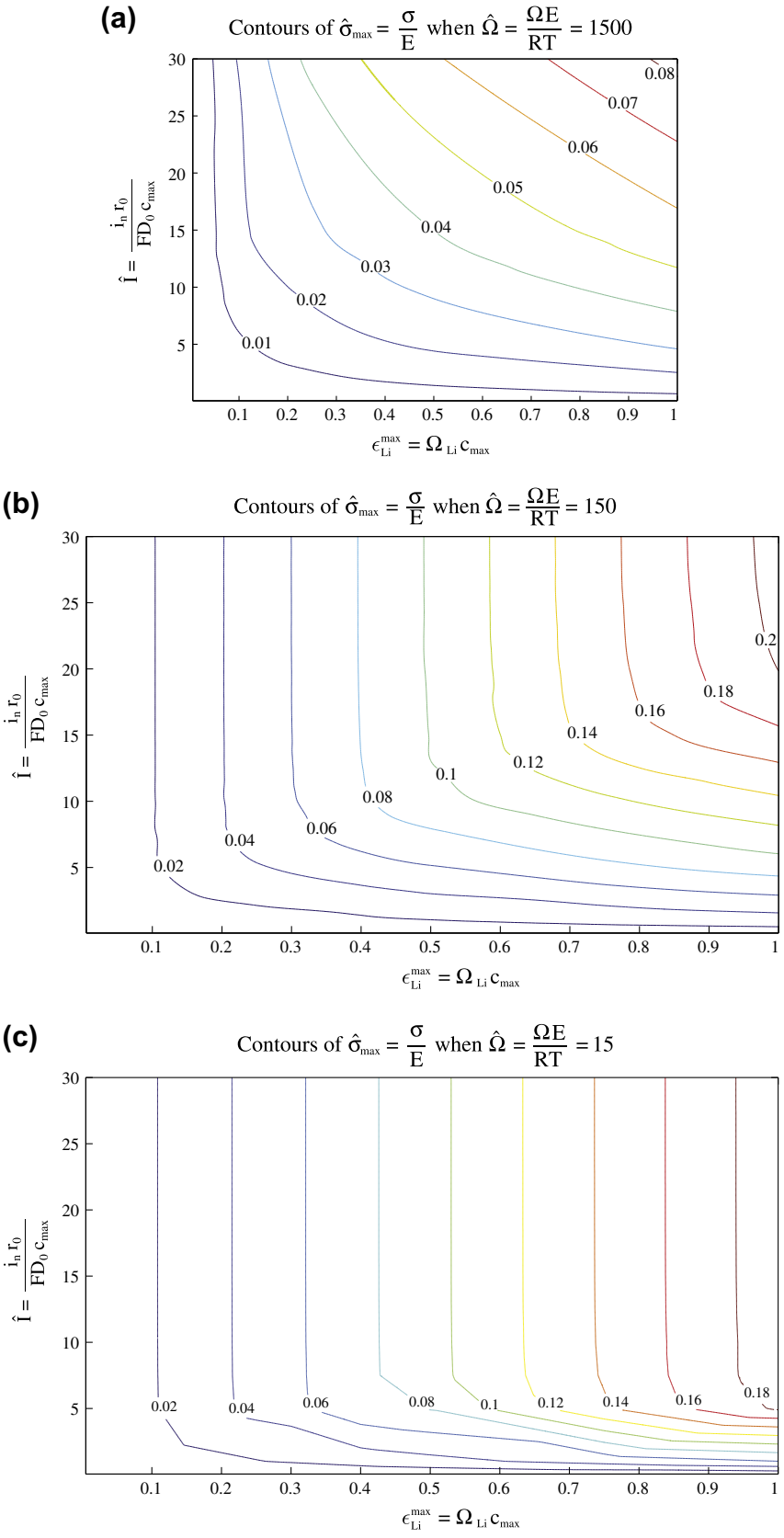

Fig. 2. Contour stress maps of the maximum stress experienced during insertion of lithium into a spherical storage particle are plotted as a function of maximum lithiation strain ϵ_{Li}^{max} and normalized insertion rate $\hat{I}$ for four values of $\hat{\Omega}$ (normalized partial molar volume) i.e. (a) $\hat{\Omega} = 1500$ (b) $\hat{\Omega} = 150$ (c) $\hat{\Omega} = 15$ (d) $\hat{\Omega} = 0$ (e) $\hat{\Omega} = 0$ (for the case of extraction).

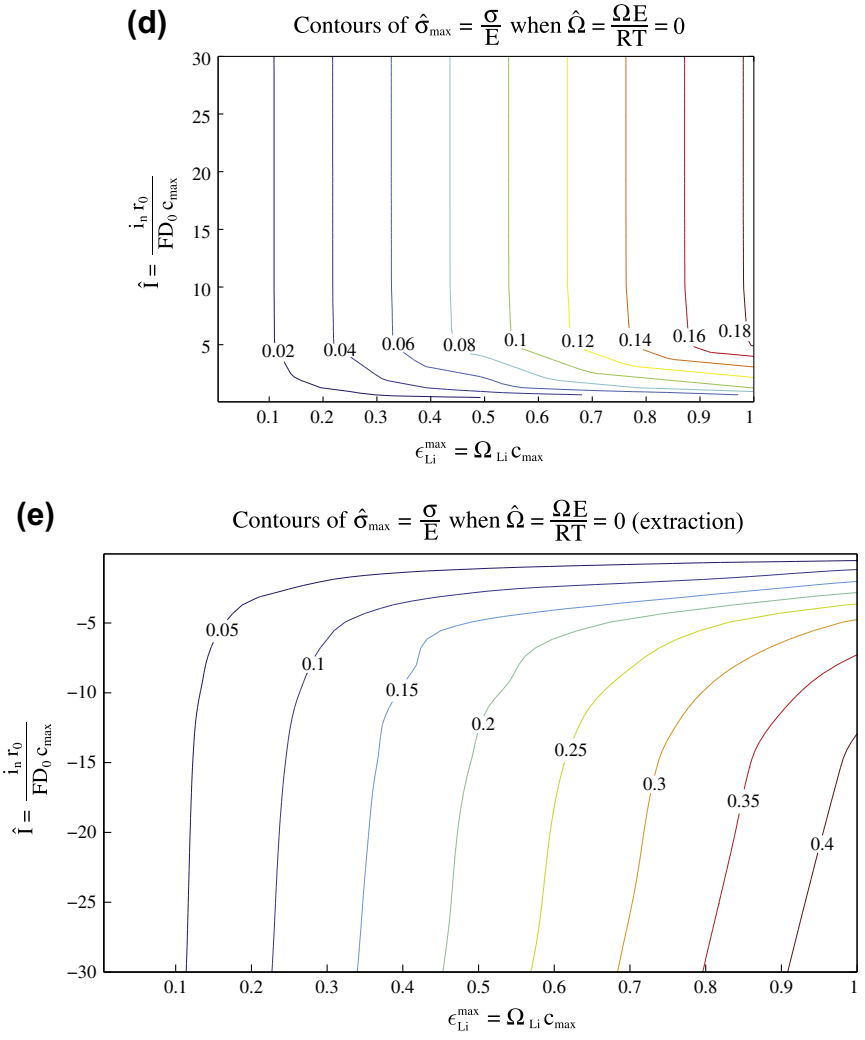

Fig. 2. (*continued*)

function of $\widehat{I}$ for spherical $Li_xMn_2O_4$ particles, with the modulus taken to be 10 GPa. Their stress results pertain to only 1 specific value of $\widehat{\Omega}$ and 1 specific value of ε_{Li}^{max}. By considering solutions for an appropriate range of values of $\widehat{I}$, $\widehat{\Omega}$ and ε_{Li}^{max} we will complement their results.

We choose an appropriate range for the parameters based on values from literature for storage particles composed of lithium manganate ($Li_xMn_2O_4$) [6,19,23];

$$D_0 = 7.08 \times 10^{-15}\ m^2/s$$
$$\Omega_{Li} = 3.497 \times 10^{-6}\ m^3/mol$$
$$E = 100\ GPa$$

Thus $\widehat{\Omega} = 141$ for $Li_xMn_2O_4$.

For a spherical particle of radius 15 μm at a surface current density of 31.3 A/m^2 the non-dimensional current is 30. Such a rate insertion corresponds to discharge at 10C, i.e. the entire particle will be filled in one-tenth of an hour or 6 min. This would be a relatively high rate of insertion or extraction for a particle, and can therefore be considered to be an upper limit.

A typical maximum upper limit for the lithium concentration in lithium manganate storage particles is $c_{max} = 2.29 \times 10^4$ mol/m^3. As a consequence, the value for ε_{Li}^{max} for Lithium Manganate is 0.08.

Taking these numbers as a baseline, a range of values extending from 0 to 1500 for $\widehat{\Omega}$, from 0.5 to 15 for $\widehat{I}$ and from 0.005 to 1.0 for ε_{Li}^{max} is selected. A strain of unity for lithiation is somewhat beyond the limit where infinitesimal strain theory is truly valid, but can be justified because new storage materials such as silicon tend to swell a great deal when they absorb lithium and the elastic strains produced when ε_{Li}^{max} is high are actually more modest. Other issues such as the distinction between undeformed and deformed configuration and its effect on the equations of mass transport that become of concern when the lithiation swelling is large have not been considered in this work.

A special note should be made for the case of $\widehat{\Omega} = 0$. This does not necessarily mean that either Young's modulus or the partial molar volume is zero. At extremely high temperatures, $T \to \infty$, $\widehat{\Omega} \to 0$, entropy driven diffusion will dominate, and the contribution of the stress gradient term in the diffusion driving force will be negligible or zero. Batteries are not operated at these high temperatures, but the case of $\widehat{\Omega} = 0$ has been included for completeness.

3. Results and discussion

The maximum tensile stress experienced by a spherical storage particle during insertion of lithium is the radial stress at the center of the particle. In Fig. 2 maps of maximum stress have been plotted as a function of dimensionless current, $\widehat{I}$, and maximum lithiation strain, ε_{Li}^{max}, for different values of $\widehat{\Omega}$. In all plots we see that the

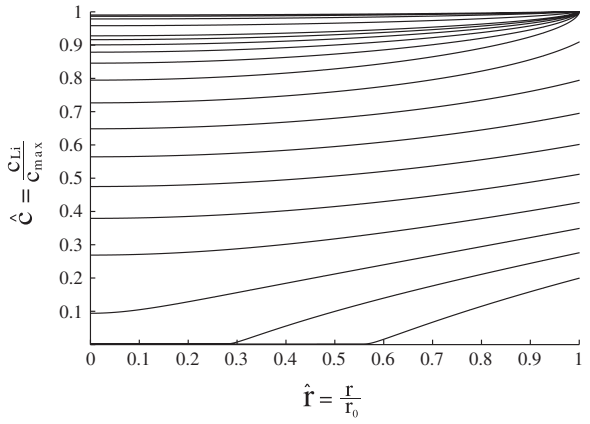

(a) Concentration profile across the particle when $\hat{I} = 30.0$, $\varepsilon_{Li}^{max} = 1.0$ and $\hat{\Omega} = 1500$

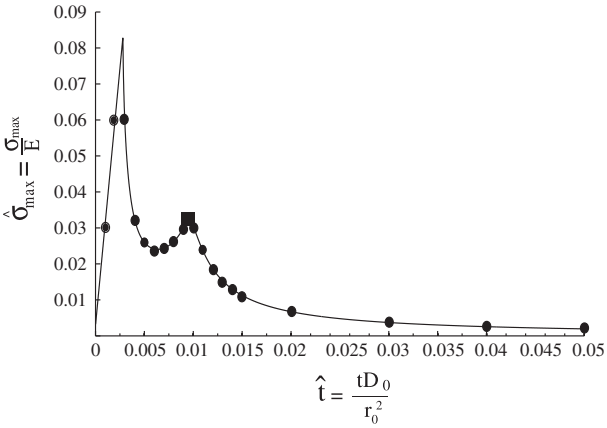

(d) Stress history over time when $\hat{I} = 30.0$ and $\varepsilon_{Li}^{max} = 1.0$ and $\hat{\Omega} = 1500$

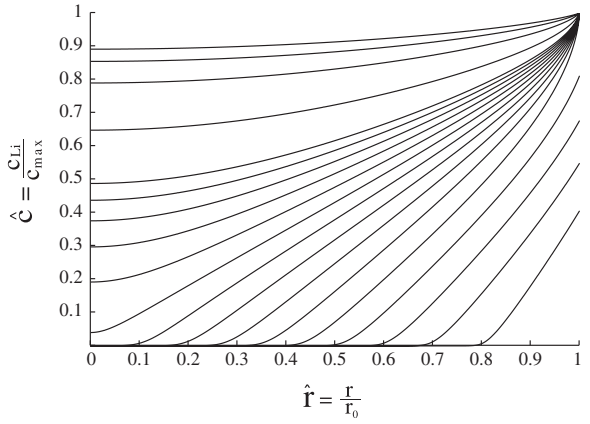

(b) Concentration profile across the particle when $\hat{I} = 30.0$, $\varepsilon_{Li}^{max} = 0.1$ and $\hat{\Omega} = 1500$

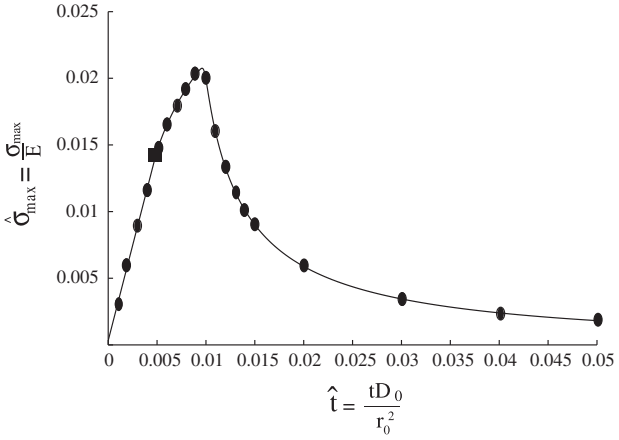

(e) Stress history over time when $\hat{I} = 30.0$ and $\varepsilon_{Li}^{max} = 0.1$ and $\hat{\Omega} = 1500$

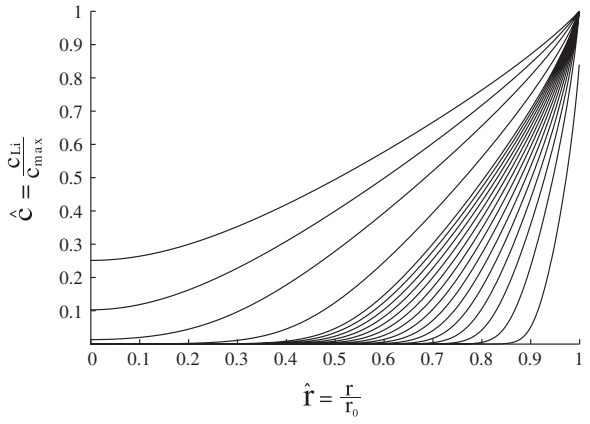

(c) Concentration profile across the particle when $\hat{I} = 30.0$, $\varepsilon_{Li}^{max} = 1.0$ and $\hat{\Omega} = 15$

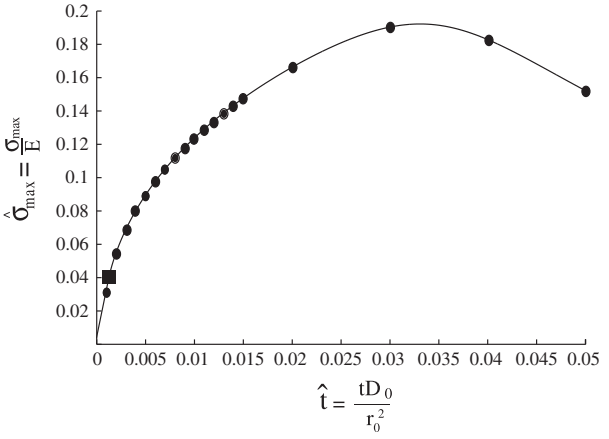

(f) Stress history over time when $\hat{I} = 30.0$ and $\varepsilon_{Li}^{max} = 1.0$ and $\hat{\Omega} = 15$

Fig. 3. Lithium concentration profiles for a spherical storage particle at specific times for particular values of normalized insertion rate $\hat{I}$, maximum lithiation strain ε_{Li}^{max} and normalized partial molar volume $\hat{\Omega}$ are plotted as a function of position within the storage particle in figures (a–c). The corresponding stress histories of maximum stress in the spherical particle are indicated by the circles in the adjoining plots in figures (d–f). (a and d) $\varepsilon_{Li}^{max} = 1.0, \hat{I} = 30$ and $\hat{\Omega} = 1500$; (b and e) $\varepsilon_{Li}^{max} = 0.1, \hat{I} = 30$ and $\hat{\Omega} = 1500$; (c and f) $\varepsilon_{Li}^{max} = 1.0, \hat{I} = 30$ and $\hat{\Omega} = 15$.

value of maximum stress increases with increasing values of $\hat{I}$ and ε_{Li}^{max}. The maximum lithiation strain ε_{Li}^{max} is the parameter that controls all strain magnitudes, including elastic ones, in the extraction or insertion process. Thus an increase in its value leads to a

monotonic increase in the value of the maximum stress. As noted by previous authors [40], the value of $\widehat{I}$ determines the concentration gradient of lithium within the storage particle, which in turn determines the value of the elastic stress. Therefore, there is a monotonic dependence of the maximum stress on the value of the dimensionless current.

The dependence of stress on $\widehat{\Omega}$ is not clearly monotonic. With a decrease in the value of $\widehat{\Omega}$ from 1500 to 150 we see an increase in the value of the maximum strain (or non-dimensionalized stress) by almost an order of magnitude, from 8% to around 20%. However, a further decrease does not lead to any further increases in the value of the stress, i.e. the value of the maximum strain seems to hold steady. This is in contrast to the almost linear dependence of stress on $\widehat{\Omega}$ as observed in stress maps for the case of extraction [41], where a decrease in the value of $\widehat{\Omega}$ leads to a monotonic increase in the value of maximum stress. Fig. 2e is a plot of a stress map generated for the case of extraction where $\widehat{\Omega} = 0$. This figure shows that the value of the maximum strain for the case of extraction reaches a maximum around 40%.

The maximum lithiation strain for lithium manganate is around 8%, and, as noted above, it has a value of $\widehat{\Omega} = 141$, so that we may consult Fig. 2c for insights into the stresses generated within such particles during insertion. If we operate a cell at high rates, e.g. $\widehat{I} = 30$ corresponding to battery discharge at 10C, the maximum stress generated is around 0.01E, or 1 GPa. During insertion, these stresses are experienced in the center of the particle, and it is unlikely that it would fracture and comminute very easily as a sizable interior flaw would have to be present to initiate the failure. However continual charging and discharging of the battery would provide conditions for small cracks to grow by fatigue, and eventual fracture and comminution of these particles even at low currents is therefore a valid concern.

We observe that the trend in maximum stress with $\widehat{\Omega}$ is that the stress rises as $\widehat{\Omega}$ falls (compare Fig. 2a–c). It seems counter-intuitive that an increase in either the partial molar volume or the Young's modulus, both components of $\widehat{\Omega}$, would lead to a decrease in the value of the maximum stress. To understand this phenomenon, we re-examine Eq. (6), the equation for flux within the particle. The stress gradient always aids the diffusion process; it is positive radially during insertion (when the radial concentration gradient is negative) and it is negative radially during extraction (when the radial concentration gradient is positive). As a result, if the value of the stress gradient is very large in comparison to the concentration gradient it can significantly affect the flux of lithium in the storage particle. The concentration gradient in turn affects the value of the stress gradient. Thus it is possible to see a strong coupling effect between the concentration and the stress gradients, depending on the values of the material parameters.

To enable a better understanding of the development of the stress, the evolution of the concentration profile across the particle is plotted in Fig. 3a–c for different values of $\widehat{I}$, $\varepsilon_{Li}^{\max}$ and $\widehat{\Omega}$. Alongside are plotted the stress profiles over time for the three cases (Fig. 3d–f). The large dots indicate the times for which the concentration profiles have been plotted. The large black square indicates the transition point; i.e. the time at which there is a transition from galvanostatic charging at the surface (constant current) to potentiostatic charging at the surface (constant concentration).

In Fig. 3a as the lithium is initially inserted into the particle, the diffusion within the particle is unable to keep up with the flux at the surface. As a result large concentration gradients develop which lead to large stresses, which can be seen in Fig. 3d. However, after an initial increase, the concentration gradient at the center starts to decrease. As the average value of the concentration increases, the value of the term $(c_{\max}-c_{Li})\,c_{Li}$ increases as well (this term reaches its maximum at $c_{Li} = 0.5$), which increases the effect of the stress gradient on the overall flux term. As a result of this, diffusion through the particle is quicker, which leads to a reduction in the concentration gradient, leading to a subsequent decrease in the value of the stress. A lower value of stress, coupled with a larger value of c_{Li} leads to an increase in the concentration gradient, and the stress starts to rise again. However, once the transition point is reached, the concentration gradient throughout the particle starts to reduce, and the stress drops.

In Fig. 3b the values of the galvanostatic current and $\widehat{\Omega}$ are kept the same as used for Fig. 3a but the value of the maximum lithiation strain, $\varepsilon_{Li}^{\max}$, is decreased by an order of magnitude. The value of the maximum stress as seen in Fig. 3d decreases, but not by an order of magnitude. This is because the decrease in $\varepsilon_{Li}^{\max}$ is compensated by an increase in the concentration and stress gradients. The concentration profile never flattens out as it did in the previous case. The concentration at the surface reaches the transition point. However, in this case the concentration gradient is much larger and the diffusive flux near the particle center is lower. Thus the concentration gradient at the center of the particle continues to increase for some time after the transition to potentiostatic charging. It is important to note that the contribution of the stress gradient term is also dependent on the value of c_{Li}, which is part of the coefficient of the stress gradient term. When the transition point is reached, the value of c_{Li} is not very high at the center of the particle, as the diffusion of lithium within the particle is relatively slow (compared to the insertion rate). Thus the contribution of the stress gradient is lower as compared to the previous scenario with the higher value of $\varepsilon_{Li}^{\max}$. This feature associated with the transition point is a very important difference from the case of extraction [41], where the transition point has an immediate effect on the concentration and stress gradient at the surface, leading to an immediate decrease in the maximum stress.

For Fig. 3c the current and maximum lithiation strain is kept the same as in Fig. 3a, however the value of $\widehat{\Omega}$ is reduced by almost two orders of magnitude to 15. As a result of this the contribution of the stress term to the overall diffusive flux is negligible, and a steep concentration gradient develops quickly. This also results in the transition point being reached more quickly than in the previous two cases, since the lithium is unable to diffuse rapidly enough from the surface into the center of the particle. Another interesting point is that the concentration gradient continues to increase for some time, until the concentration of lithium at the center becomes slightly greater than zero.

The fact that the maximum stress is experienced some time after the transition point is reached would also explain why the maximum stress as seen in Fig. 2 maintains the same value as $\widehat{\Omega}$ is reduced below 15. When $\widehat{\Omega}$ has a low value, the transition point is reached quickly. As a result, the concentration gradient at the center of the particle becomes invariant across the different cases, since the value of c_{Li} is always close to $c_{\max}$ at the surface and 0 at the center. Depending on the distribution of lithium within the particle at the transition point, the time taken to reach the maximum stress at the center differs, but the value of the maximum stress essentially remains the same.

In Fig. 4 the stress histories for different values of $\widehat{\Omega}$ are plotted for specific values of $\widehat{I}$ and $\varepsilon_{Li}^{\max}$. The black dots indicate the time at which the transition from galvanostatic charging to potentiostatic charging is reached. In Fig. 4a, the effect of high values of $\widehat{\Omega}$ is to reduce the value of the maximum stress. More importantly the double-peaked shape of the stress profile is only seen for high combinations of $\widehat{\Omega}$ and $\varepsilon_{Li}^{\max}$. At lower values the profile shows a single peak only. It can be seen that the time at which the transition point is reached decreases as the value of $\widehat{\Omega}$ is decreased. The reason is that when the value of $\widehat{\Omega}$ is decreased, the contribution of the stress gradient to the overall flux term decreases, leading to a large concentration gradient. Mass accumulates closer to the surface and does not diffuse into the particle quickly. As a result the surface

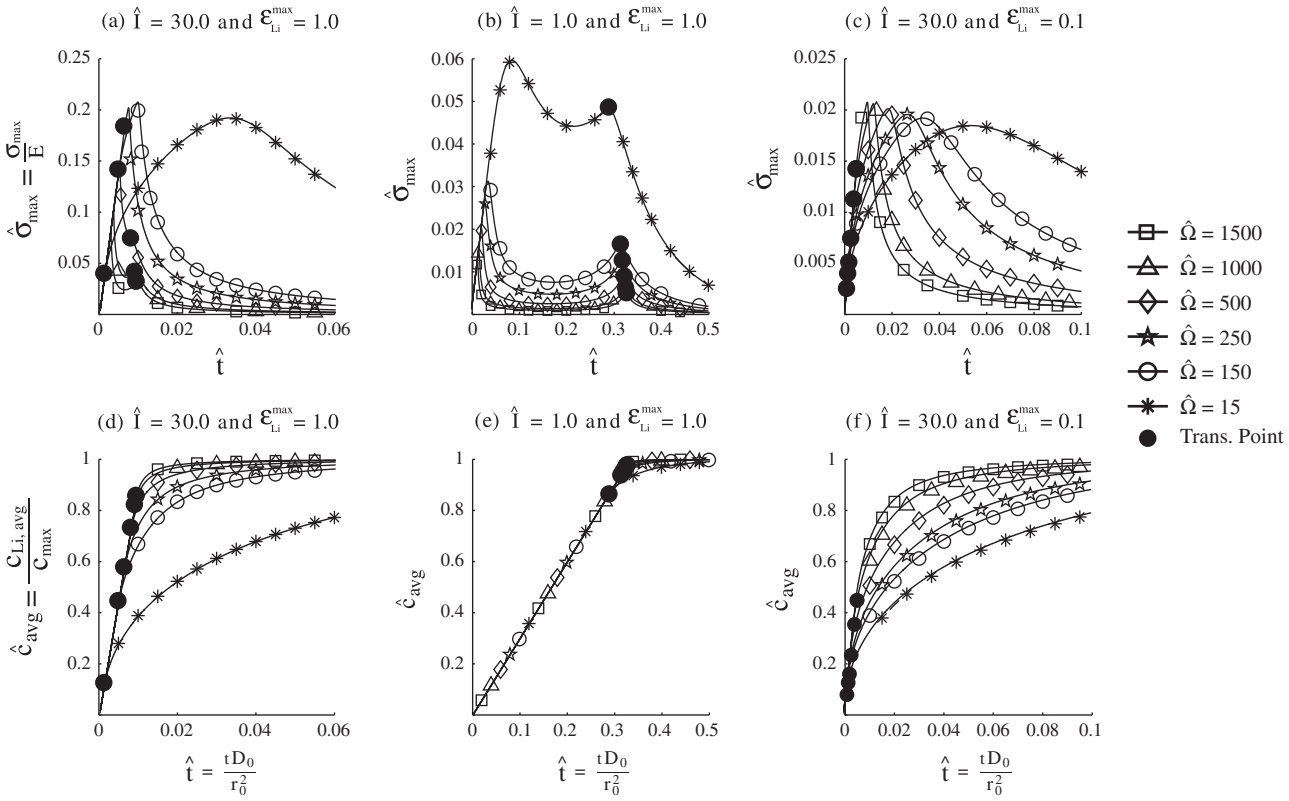

Fig. 4. Histories of maximum principal stress (a–c) and average lithium concentration (SOC) (d–f) in a storage particle during galvanostatic insertion followed by potentiostatic insertion. Different combinations for normalized partial molar volume $\widehat{\Omega}$, maximum lithiation strain ε_{Li}^{max} and normalized insertion rate $\widehat{I}$ are chosen. Each plot shows the influence of changing the normalized partial molar volume $\widehat{\Omega}$. The values of the parameters are as follows: (a and d) $\varepsilon_{Li}^{max} = 1.0$ and $\widehat{I} = 30$; (b and e) $\varepsilon_{Li}^{max} = 1.0$ and $\widehat{I} = 1.0$; (c and f) $\varepsilon_{Li}^{max} = 0.1$ and $\widehat{I} = 30$.

reaches the maximum value of concentration much earlier, triggering the transition in the boundary conditions. The profile for $\widehat{\Omega} = 15$ stands out due to the fact that the peak stress is reached more gradually. This is because the transition point is reached early. The mass of lithium within the particle takes time to redistribute evenly; i.e. the concentration profile takes time to flatten out. Thus the development of the stress profile is also more gradual. However, the value of the maximum stress does not vary much for the lower values of $\widehat{\Omega}$.

Fig. 4d shows the average concentration of lithium within the particle as a function of time; i.e. the SOC. It can be seen that for higher values of $\widehat{\Omega}$ the SOC is much higher at the transition point. The reason is the same as described earlier; large values of $\widehat{\Omega}$ lead to flatter concentration profiles. Thus more lithium can be distributed evenly within the particle, even at relatively higher charging rates, before transition is reached. As the values of $\widehat{\Omega}$ decrease and the transition point is reached later, the particle takes longer to fill up. This is because the diffusive flux within the particle is not large enough to redistribute the lithium quickly. The SOC plots as a function of time reflect this fact.

In Fig. 4b the dimensionless current is reduced from $\widehat{I} = 30$ to $\widehat{I} = 1$. Since the flux at the surface is reduced, the concentration gradient within the particle reduces as well, leading to an overall decrease in the maximum stress in the particle. However, unlike the previous case, even lower values of $\widehat{\Omega}$ have an effect on the value of stress. Since the overall concentration gradient is lower, the stress gradient does not have to be very high in order to have an effect on the overall diffusive flux. As a result we see a double peak in the stress history for all values of $\widehat{\Omega}$. The plots of SOC versus time in Fig. 4e show that the average concentration develops similarly across all values of $\widehat{\Omega}$ until the transition point is reached. After this point, depending on the value of $\widehat{\Omega}$ and the subsequent value of the diffusive flux, lithium diffuses within the particle at differing rates, with higher values of $\widehat{\Omega}$ showing flatter profiles.

Finally in Fig. 4c we see stress histories for $\widehat{I} = 30$ but in this case the value of ε_{Li}^{max} is reduced to 0.1. There is an overall decrease in the value of the maximum stress experienced, since ε_{Li}^{max} influences the value of the stress monotonically. We see only a single peak for the stress: the value of the stress gradient is not large enough to affect the concentration gradient. As a result we see that the transition points are reached rather quickly for all cases of $\widehat{\Omega}$ and the value of the maximum stress does not change much with $\widehat{\Omega}$.

In order to look at the way stress histories develop for the different cases of insertion and extraction, the stress histories for the two different cases are plotted in Fig. 5. For this figure, material parameters similar to those for lithium manganate are considered, i.e. $\widehat{\Omega} = 150$ and $\varepsilon_{Li}^{max} = 0.1$, and the values of the dimensionless current $\widehat{I}$ are varied. The main figure contains the plots for $\widehat{I}$ ranging from 5 to 30 while the inset contains the plots for $\widehat{I}$ from 0.05 to 1. As $\widehat{I}$ decreases the value of the maximum stress decreases, which is in line with earlier results. Stress histories at lower values of $\widehat{I}$ also show a double peak in time. This is expected given that at lower currents, the stress gradient term will be able to make a larger contribution to the overall diffusive flux. The plots for higher values of currents show that the particle experiences larger stresses during extraction (Fig. 5b) than during insertion (Fig. 5a). It is important to remember that for extraction, the maximum tensile stress occurs at the surface of the particle. Hence any changes in the boundary condition is reflected immediately in the stress history. Thus for extraction, after the transition point is reached the maximum stress immediately drops, whereas it continues to rise

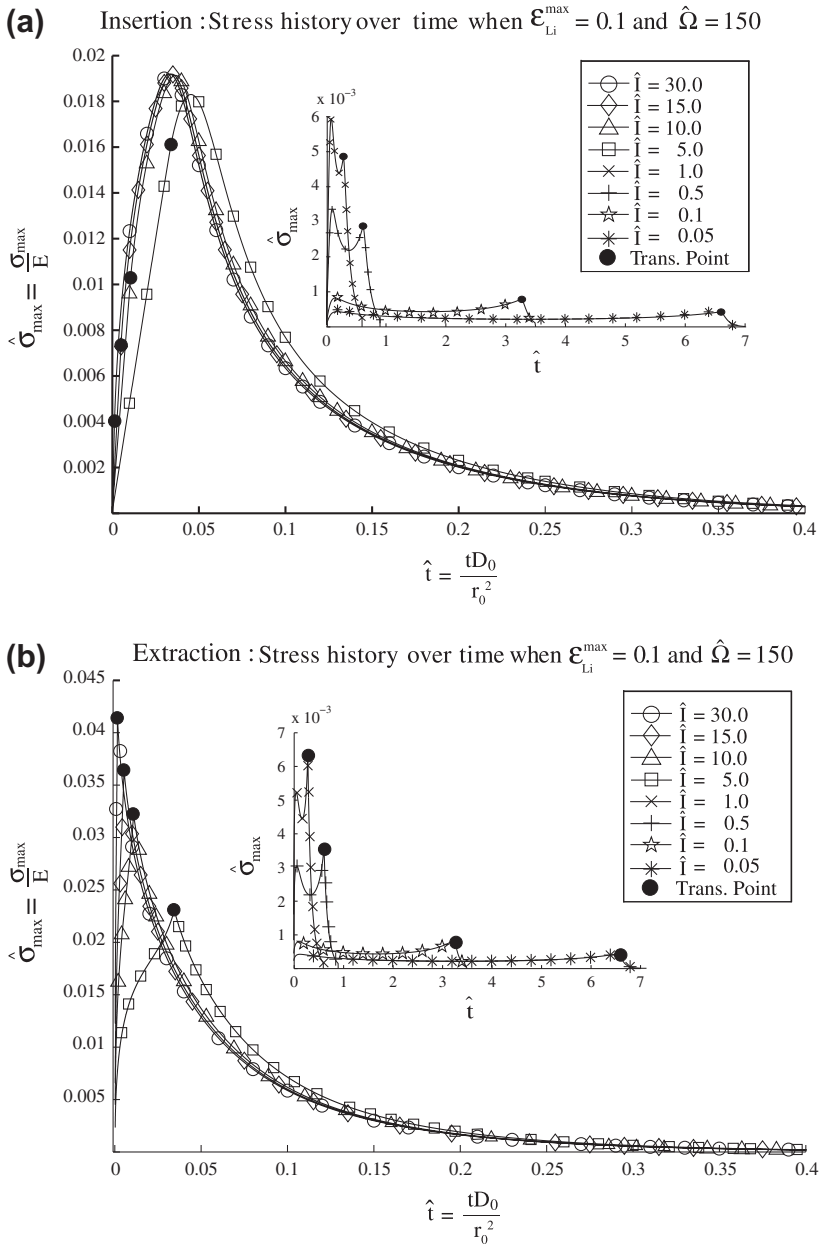

Fig. 5. Comparison of stress and SOC histories for the case of insertion and extraction of lithium into a spherical storage particle. Initially, the particle is charge galvanostatically and then it is charged potentiostatically when the relevant boundary condition is achieved at the surface of the particle. The material parameters chosen are close to those of lithium manganate; i.e. maximum lithiation strain $\varepsilon_{Li}^{max} = 0.1$ and $\widehat{\Omega} = 150$. In all of the figures, the larger graph contains plots for $\widehat{I} = 5, 10, 15, 30$, while the inset plot is for $\widehat{I} = 1.0, 0.5, 0.1, 0.05$. (a) A plot of stress histories for the case of insertion. (c) A plot of the corresponding SOC histories for the case of insertion. (b) A plot of stress histories and (d) of SOC histories for the case of extraction.

in the case of insertion. More importantly this is also the reason why the values of the stress maximum are not monotonic in $\widehat{\Omega}$ in the case of insertion. The extremely high gradients formed at the surface of the particle take time to translate to the center, which is where maximum stress occurs during insertion. In most cases, the transition point is reached before the gradient of the lithium concentration at the center is developed. Hence we see that the stress history continues to evolve after the transition point during insertion, and that the magnitude of stress is not as high as in extraction.

For the lower values of current, the values of stress are comparable for the cases of extraction and insertion. The plots for insertion for these currents as seen in the inset in Fig. 5a indicate that the stress starts to decrease almost immediately after the transition point is reached. This is because, for these cases, the concentration profile within the particle is relatively flat, and the concentration gradient also develops more quickly across the particle. Therefore changes in conditions at the particle surface are reflected more rapidly by developments at the particle center. When the insertion and extraction current is low, the stress histories display a double peak in time. However, in the case of insertion, the second peak in the maximum stress is not as high as the first one, in contrast to the case of extraction. This is most probably because the concentration gradient at the center is not maximized before the transition point is reached.

Fig. 5c–d shows the histories for the SOC for different values of insertion and extraction current, with the insets showing the plots for lower values of current. The shapes of the curves for extraction are quite similar to each other, as are those for insertion.

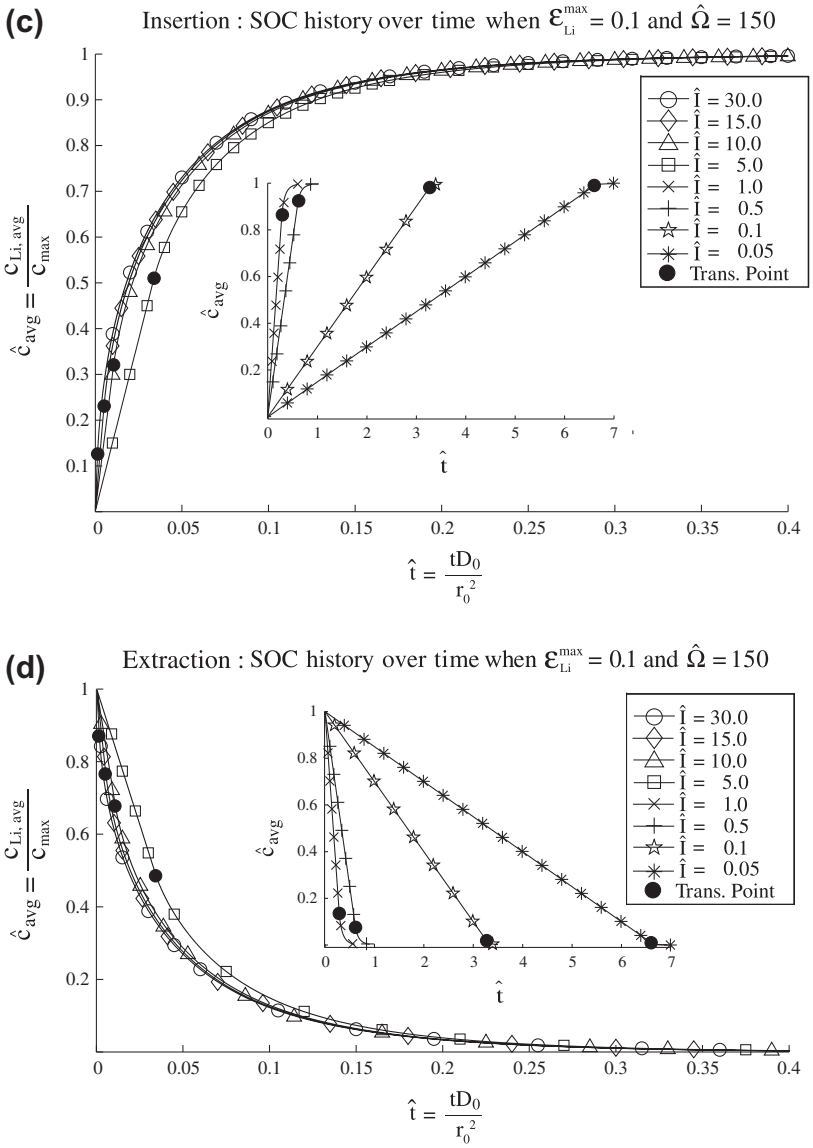

Fig. 5. (*continued*)

Finally, for the sake of completeness, plots of the stress history during insertion are shown in Fig. 6, with the effect of varying ε_{Li}^{max} illustrated. Since the results are similar to those shown previously, we make no attempt to describe the features of these figures.

We now comment on some features of stress generation in storage particles, some of them well known. Our results show that high values of dimensionless current during lithium extraction cause larger tensile stresses than during insertion. At lower currents, the values of maximum stress for the cases of insertion and extraction are similar. During extraction, the maximum stresses occur at the particle surface, whereas during insertion they occur at the center of the particle. Thus if a battery were cycled, it would be during extraction of lithium that cracks would grow, the assumption being that pre-existing cracks are found preferentially at the surface. Nevertheless, the values of the maximum stresses in both insertion and extraction are large enough to be of concern and are potentially large enough to cause particle fracture and comminution.

The results also indicate that certain materials might be better suited to charging at fast rates than others with respect to the stress developed within the particle. High values of $\widehat{\Omega}$ and ε_{Li}^{max} help to increase the effect of the stress gradient on the lithium flux rate, tending to reduce the lithium concentration gradients and thus the peak maximum stress. A double peaked stress history is seen for high values of these parameters as well, which is also an effect of the term $c_{Li}(1 - c_{Li}/c_{max})$. This limits the contribution of the stress gradient to the diffusive flux at the limiting values of concentration, leading to sluggish diffusion rates and increased lithium concentration gradients. The reduced effect of the stress at extreme values of concentration is a result of the formulation of the chemical potential as given in Eq. (1), because the entropic contribution term $RT \ln [c_{Li}/(c_{max} - c_{Li})]$ dominates. Thus the diffusion equation becomes similar to that of Fickian diffusion. This is a result of considering an idealized material, with no interaction effects or phase changes. Conway [42] comment that some materials such as Li_xTiS_2 exhibit free energy curves that are very close to these idealized "Langmuir" contours.

It is important to note that part of the prefactor arises from the concentration dependent mobility. If we assume that the mobility is concentration independent, then we arrive at the formulation of Zhang et al. [19]. For this formulation, in the case of insertion, stress will not contribute to the diffusive flux initially, and one

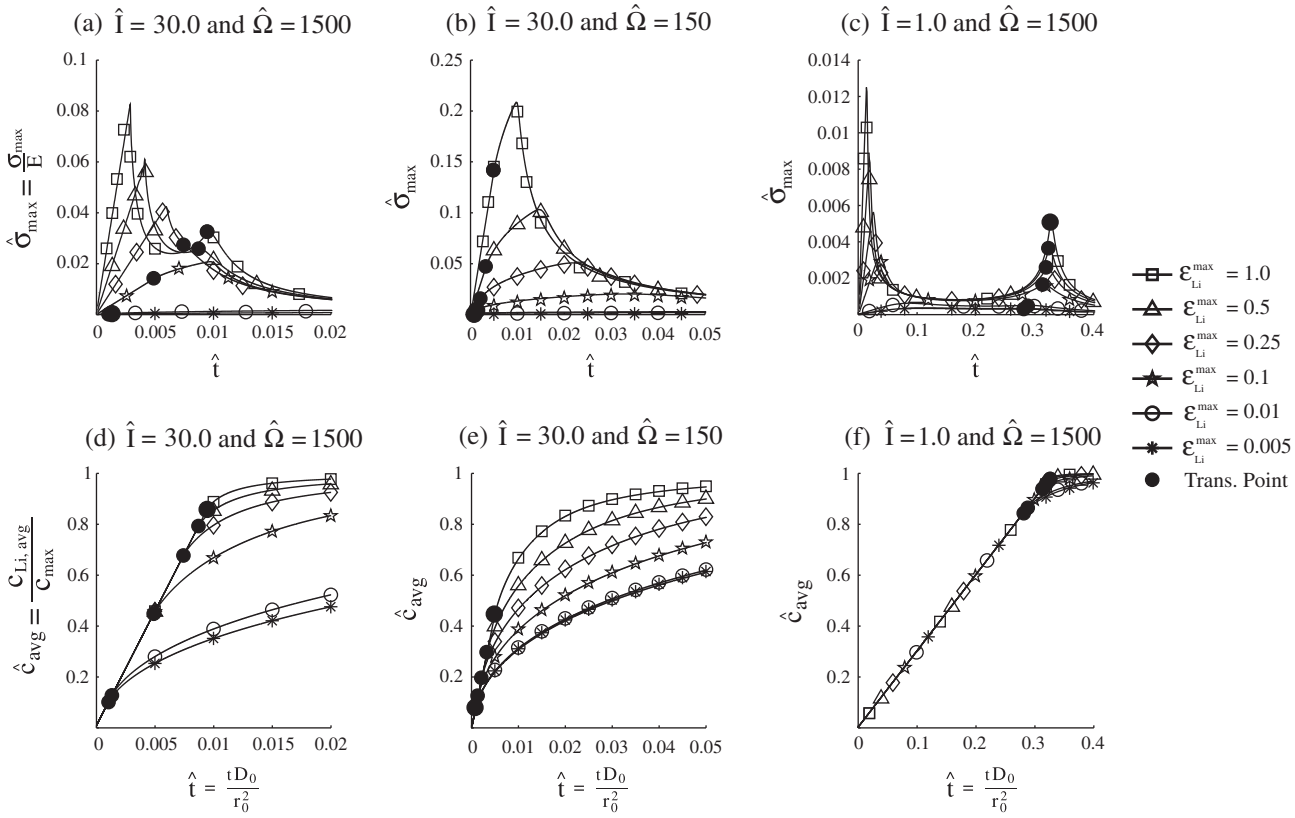

Fig. 6. Histories of maximum principal stress (a–c) and average lithium concentration (SOC) (d–f) in a storage particle during galvanostatic insertion followed by potentiostatic insertion. Different combinations for normalized partial molar volume $\widehat{\Omega}$, maximum lithiation strain $\varepsilon_{Li}^{\max}$, and normalized insertion rate $\widehat{I}$ are chosen. Each plot shows the influence of changing the value of the maximum lithiation strain $\varepsilon_{Li}^{\max}$. The values of the parameters are as follows: (a and d) $\widehat{I} = 30$ and $\widehat{\Omega} = 1500$; (b and e) $\widehat{I} = 30$ and $\widehat{\Omega} = 150$; (c and f) $\widehat{I} = 1.0$ and $\widehat{\Omega} = 1500$.

would expect to see a peak followed by a flattening out of the curve. For extraction while initial concentration gradients might cause a slight peak, the net effect would be a decreasing contribution of the stress to the diffusive flux at the surface as the concentration decreases, leading to a rise in stress. We can consider this in terms of an effective diffusion coefficient, which considers the effect of the stress gradients as well as the concentration gradients. For the concentration independent mobility, the effective diffusion coefficient will rise as the concentration increases. However, as intercalation sites fill up, leaving fewer vacancies for lithium ions to intercalate into, one would expect diffusion in the system to decrease. Therefore one needs to include a concentration dependent term in the equation for mobility. This also helps to create symmetry in the effect of the hydrostatic stress gradient with respect to the concentration.

The effective value of the dimensionless current $\widehat{I}$, can be reduced by choosing small particles or a material with a large coefficient of diffusion. However when storage particles are first exposed to the electrolyte, often a film forms on the surface, known as the solid electrolyte interface (SEI), consuming active storage material and reducing the battery capacity [2–5]. As a consequence, when very small storage particles are used, a large fraction of the active storage material is lost due to the SEI formation, undermining the advantage of using small storage particles. This feature is just one example of the fact that a battery system involves many parameters that must be optimized simultaneously within constraints for maximal performance to be achieved.

The results we have provided are for an idealized case of a spherical particle. Most images of storage particles indicate that the shapes are not spherical, displaying many facets and irregularities. The presence of sharp re-entrant corners will influence the concentration of stress within the particle, causing them be more prone to fracture and comminution. Given the coupling between diffusion and stress, it is likely to be important to investigate how the lithium concentration gradient develops at sharp, re-entrant corners, and how that influences the maximum stresses that are generated.

4. Conclusion

A model for diffusion of lithium in storage particles has been developed. A non-dimensionalized set of equations was implemented with three important non-dimensional parameters, the dimensionless current, $\widehat{I}$, the maximum lithiation strain, $\varepsilon_{Li}^{\max}$, and the non-dimensional partial molar volume, $\widehat{\Omega}$. Stress maps for the case of insertion and extraction in a spherical particle were developed and show that the parameter $\widehat{\Omega}$ has an inverse effect on the value of maximum stress. This is due to the effect that $\widehat{\Omega}$ has on the contribution of the stress gradient to the overall diffusive flux, seen in the development of the concentration profile across the particle. A comparison was made between the cases of insertion and extraction, showing that at higher currents, extraction generates higher stresses in the particle than does insertion. Since during extraction the maximum tensile stress is experienced at the surface of the particle rather than at its center, there is a greater possibility of cracks growing during extraction, leading to particle fracture and comminution. Nevertheless, the stresses generated during insertion are significant enough to contribute towards particle fracture and comminution.

By developing a non-dimensionalized set of parameters, we are able to highlight clearly the effects of the different material and

system properties on the overall behavior of the system, including the generation of stress within storage particles. The results confirm the highly-coupled nature of lithium concentration and stress within the particle. Although simplifying assumptions have been made, our model enables insights to be obtained regarding the behavior of lithium storage particles during battery charging and discharging. We note also that our model can be applied to a variety of materials by choice of the appropriate values of the three different dimensionless parameters, $\epsilon_{Li}^{\max}$, $\widehat{I}$ and $\widehat{\Omega}$.

Acknowledgments

The research in this paper is supported by a contract with the Robert Bosch Corporation and a grant from the University of California Discovery Program. We thank Esther Bohn and Thomas Eckl from Robert Bosch GmbH, Stuttgart, Germany for stimulating discussions and valuable comments.

References

[1] USABC 'Goals for Advanced Batteries for EV's'. <http://www.uscar.org/guest/article_view.php?articles_id=85> (last accessed 9.10.11).
[2] R.A. Huggins, Advanced Batteries: Materials Science Aspects, Springer Science+Business Media, New York, 2009.
[3] J. Vetter, P. Novak, M.R. Wagner, C. Veit, K.-C. Moeller, J.O. Besenhard, M. Winter, M. Wohlfahrt-Mehrens, C. Vogler, A. Hammouche, Journal of Power Sources 147 (2005) 269–281.
[4] J.-M. Tarascon, M. Armand, Nature 414 (2001) 359–367.
[5] G.-A. Nazri, G. Pistoia (Eds.), Lithium Batteries: Science and Technology, Kluwer, 2004.
[6] J. Christensen, J. Newman, Journal of the Electrochemical Society 153 (2006) A1019–A1030.
[7] J.O. Besenhard, Handbook of Battery Materials, Wiley-VCH, 1998.
[8] J. Christensen, J. Newman, Journal of Solid State Electrochemistry 10 (5) (2006) 293–319.
[9] K.E. Thomas, R.M. Darling, J. Newman, Mathematical modeling of lithium batteries, in: W. van Schalkwijk, B. Scrosati (Eds.), Advances in Lithium-Ion Batteries, Kluwer AcademicPlenum Publishers, 2002, pp. 345–392.
[10] M. Doyle, T.F. Fuller, J. Newman, Journal of the Electrochemical Society 140 (1993) 1526–1533.
[11] M. Doyle, J. Newman, A. Gozdz, C. Schmutz, J.M. Tarascon, Journal of the Electrochemical Society 143 (1996) 1890–1903.
[12] S. Devan, V.R. Subramanian, R.E. White, Journal of the Electrochemical Society 152 (2005) A947–A955.
[13] G. Ning, R.E. White, B.N. Popov, Electrochimica Acta 51 (2006) 2012–2022.
[14] D.E. Stephenson, E.M. Hartman, J.N. Harb, D.R. Wheeler, Journal of the Electrochemical Society 154 (2007) A1146–A1155.
[15] S. Renganathan, G. Sikha, S. Santhanagopalan, R.E. White, Journal of the Electrochemical Society 157 (2010) A155–A163.
[16] J. Christensen, Journal of the Electrochemical Society 157 (2010) A366–A380.
[17] R.E. Garcia, Y.-M. Chiang, W.C. Carter, P. Limthongkul, C.M. Bishop, Journal of the Electrochemical Society 152 (2005) A255–A263.
[18] R.E. Garcia, Y.-M. Chiang, Journal of the Electrochemical Society 154 (2007) A856–A864.
[19] X. Zhang, W. Shyy, A.M. Sastry, Journal of the Electrochemical Society 154 (2007) A910–A916.
[20] J. Park, W. Lu, A.M. Sastry, Journal of the Electrochemical Society 158 (2011) A201–A206.
[21] Y.-T. Cheng, M.W. Verbrugge, Journal of the Electrochemical Society 157 (2010) A508–A516.
[22] Y.-T. Cheng, M. Verbrugge, Journal of Power Sources 190 (2009) 453–460.
[23] E. Bohn, Partikel-Modell fur Lithium-Diffusion und mechanische Spannungen einer Interkalationselektrode, PhD thesis, Karlsruhe Institute of Technology, 2012.
[24] E. Markervich, G. Salitra, M.D. Levi, D. Aurbach, Journal of Power Sources 146 (2005) 146–150.
[25] H. Gabrisch, J. Wilcox, M.M. Doeff, Electrochemical and Solid-State Letters 11 (3) (2008) A25–A29.
[26] S.J. Harris, R.D. Deshpande, Y. Qi, I. Dutta, Y.-T. Cheng, Journal of Materials Research 25 (8) (2010) 1433–1440.
[27] J. Li, A.K. Dozier, Y. Li, F. Yang, Y.-T. Cheng, Journal of the Electrochemical Society 158 (6) (2011) A689–A694.
[28] M.W. Verbrugge, B.J. Koch, Journal of the Electrochemical Society 143 (2006) 600–608.
[29] K.E. Aifantis, J.P. Dempsey, Journal of Power Sources 143 (2005) 203–211.
[30] K. Zhao, M. Pharr, J.J. Vlassak, Z. Suo, Journal of Applied Physics 108 (2010) 073517-1–073517-6.
[31] F. Yang, Journal of Applied Physics 108 (2010) 073536-1–073536-5.
[32] Y.-T. Cheng, M.W. Verbrugge, Electrochemical and Solid State Letters 13 (2010) A128–A131.
[33] W.H. Woodford, Y.-M. Chiang, W.C. Carter, Journal of the Electrochemical Society 157 (2010) A1052–A1059.
[34] T.K. Bhandakkar, H. Gao, International Journal of Solids and Structures 47 (2010) 1424–1434.
[35] T.K. Bhandakkar, H. Gao, International Journal of Solids and Structures 48 (2011) 2304–2309.
[36] Y. Hu, X. Zhao, Z. Suo, Journal of Materials Research 25 (6) (2010) 1007–1010.
[37] G.G. Botte, R.E. White, Journal of the Electrochemical Society 148 (2001) A54–A66.
[38] S.P. Timoshenko, J.N. Goodier, Theory of Elasticity, second ed., McGraw-Hill, 1951.
[39] Comsol Multiphysics User's Guide, Version 3.5a, November 2008.
[40] F. Yang, Materials Science and Engineering A 409 (2005) 153–159.
[41] R. Purkayastha, R. McMeeking, Journal of Applied Mechanics 79 (2012) 031021-1–031021-16.
[42] B.E. Conway, Electrochimica Acta 38 (9) (1993) 1249–1258.